Supporting information

Airborne metal nanoparticles released by azides detonation: determination and potential public exposure.

Tianyu Cen[1,2], Zheyu Zhang[3], Laura Torrent[1,4], Elisabeth Müller[5], Christian Ludwig[1,2], Andrea Testino[1,6]*

[1]Laboratory for Sustainable Energy Carriers and Processes (LEP), Paul Scherrer Institut (PSI), Villigen PSI 5232, Switzerland

[2]Environmental Engineering Institute (IIE, GR-LUD), School of Architecture, Civil and Environmental Engineering (ENAC), École Polytechnique Fédérale de Lausanne (EPFL), Lausanne 1015, Switzerland

[3]Electrochemistry Laboratory (LEC), Paul Scherrer Institut (PSI), Villigen PSI 5232, Switzerland

[4]Department of Chemistry, Faculty of Sciences, University of Girona (UdG), Girona 17004, Spain

[5]Laboratory of Nanoscale Biology (LNB), Paul Scherrer Institut (PSI), Villigen PSI 5232, Switzerland

[6]STI SMX-GE, École Polytechnique Fédérale de Lausanne (EPFL), Lausanne 1015, Switzerland

*Corresponding authors: andrea.testino@psi.ch

Contents

1. Direct particle collection for TEM analysis

To investigate the airborne particles without manipulation, the analytical setup can be modified according to Figure S1. In such a configuration, a transmission electron microscopy (TEM) grid (Au 400 mesh 1.2/1.3, Quantifoil, Germany) is placed in a dedicated holder operated as described in previous works[1,2]. The metallic particles carried by the Ar stream are fractionated in the DMA and trapped directly on the TEM grid for analysis. The Ar flow rate is set to 0.9 L/min and the sampling time to 30 min. Alternatively, the DMA can be omitted, and the full particle size distribution collected on the TEM grid.

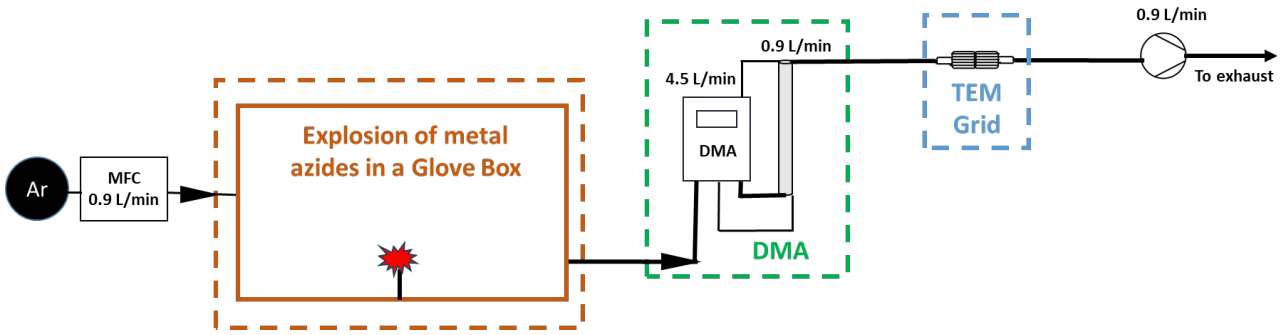

Figure S1 - Schematic representation of the proposed method for collecting offline NPs on a TEM grid after the explosion of metal azides in a glove box.

After the offline collection, the particles were analyzed by TEM (Joel JEM-ARM 200F, Japan) operating at 200 KV. A high-angle annular dark field detector (HAADF) was used for scanning transmission electron microscopy (STEM) imaging. Energy dispersive X-ray (EDX) analysis was performed over 1000 s at a beam current of 130 pA. STEM-EDX maps and EDX spectra were acquired, in order to qualitatively identify the composition of the particles (Ag, Cu and AgCu alloy).

2. Energy dispersive X-ray (EDX) analysis

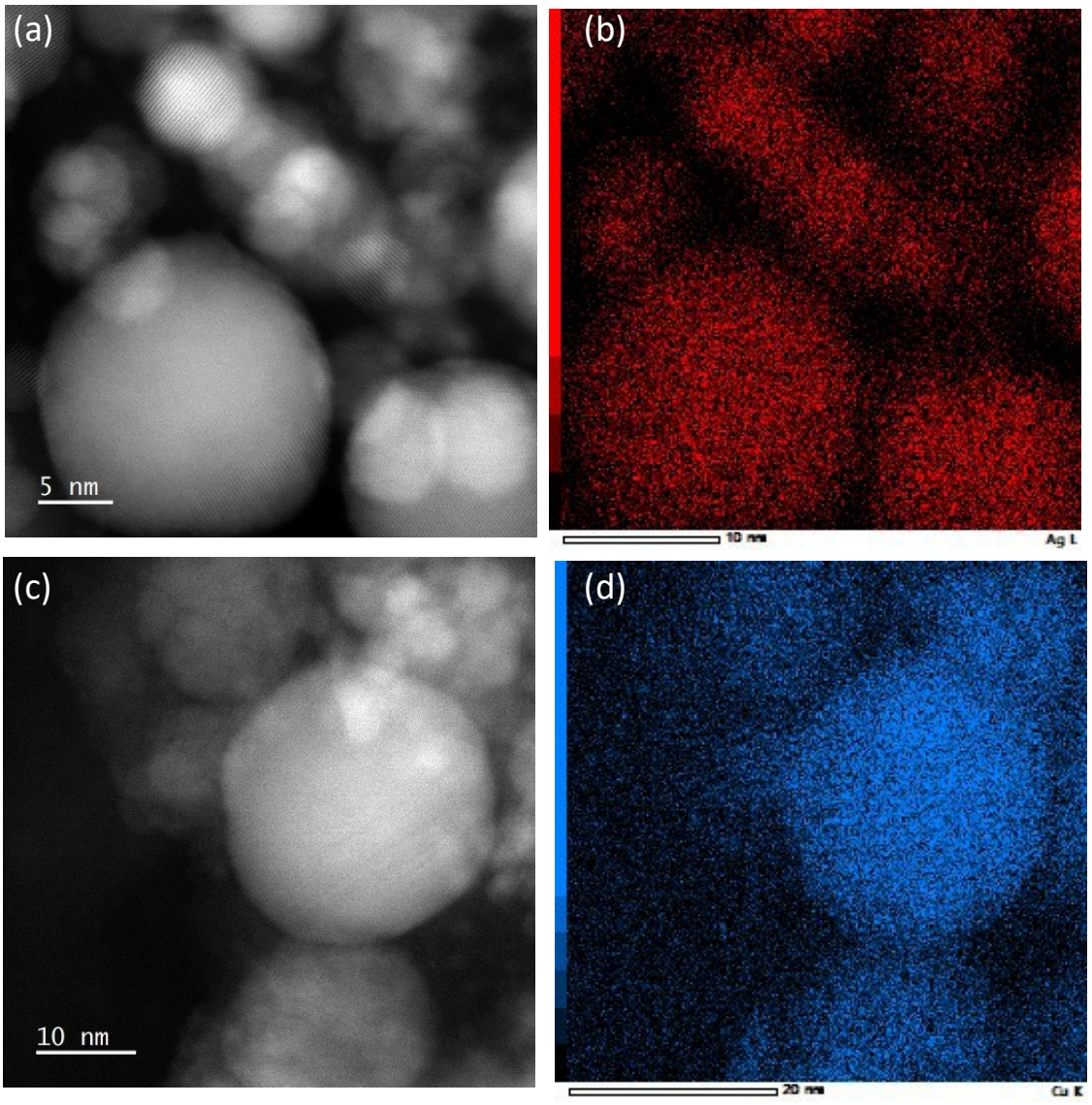

Figure S2 – HAADF STEM images of NPs collected offline after the explosion of AgN_3 (a) and CuN_6 (c), respectively, in the glove box. STEM-EDX maps at the Ag L-edge (b) and Cu K-edge (d).

High-resolution TEM – single metal

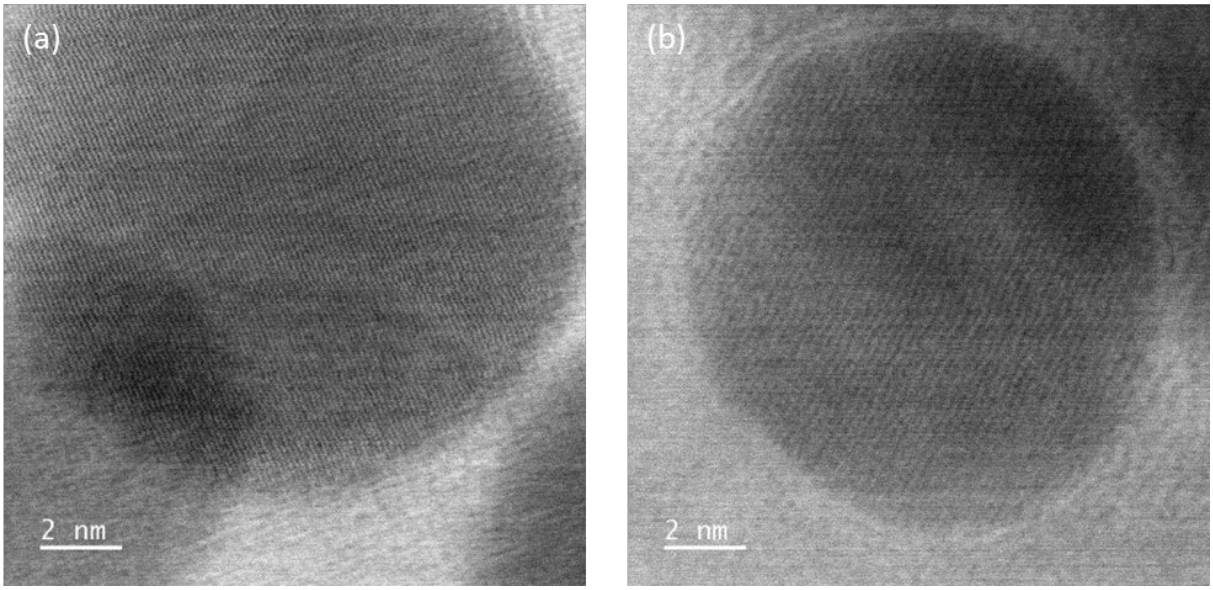

Figure S3 – High-resolution TEM images of NPs collected offline after the explosion of AgN_3 (a) and CuN_6 (b) in the glove box (bright-field).

3. Setup validation for online measurement

Before running the experiment with the unknown particles generated from the explosion, the setup of the glovebox coupled to RDD-spICP-MS was calibrated using standard nanoparticles. As shown in Figure S4, the setup could run in association (top) and decay (bottom) mode.

In association mode, the whole glove box was flushed with argon before use, keeping the oxygen concentration below 0.2%. The standard AgNP suspension containing 100 nm NPs purchased from Nanocomposix (USA) was diluted into 5×10^6 #/mL by Milli-Q water in the bottle of an aerosol generator (AG, TOPAS ATM220, Germany). An AG operated with argon was used to generate the metallic NP aerosol and maintain a flow rate of 0.9 L/min. The aerosol flow first passed through a silica gel dryer column to remove the water and was finally injected into the glove box. After starting the aerosol generation, the spICP-MS would start to measure the NPs at the time interval of 5 min. For each measurement, it recorded the data for 2 min and finally summarized the PSD and PNC based on the same data treatment methods followed in previous studies[3,4]. The DR in RDD will be adjusted based on the last measurement to make sure the PNC at each measurement will always stay inside the optimal PNC range (between 50 and 1000 particles per minute in spICP-MS). In theory, the NP concentration inside the glove box and transferred to RDD-spICP-MS will follow the one-phase association process, which is presented in **Equation S1**.

$$\frac{dC}{dt} = (C_{in} - C)\frac{Q}{V} \qquad \textbf{Equation S1}$$

Where C is the number concentration of NPs inside the glove box and transferred to RDD-spICP-MS. C_{in} is the number concentration of NPs in the aerosol generated after the AG. Q is the flow rate of the aerosol, which is always at 0.9 L/min in this project. V is the volume of the glove box when the NPs were homogeneously mixed inside the glove box. After the integration

of the time, the time-resolved number concentration of NPs in the glove box could be expressed as **Equation S2**.

$$C = C_{in} \times (1 - e^{-\frac{Q}{V}t}) \qquad \textbf{Equation S2}$$

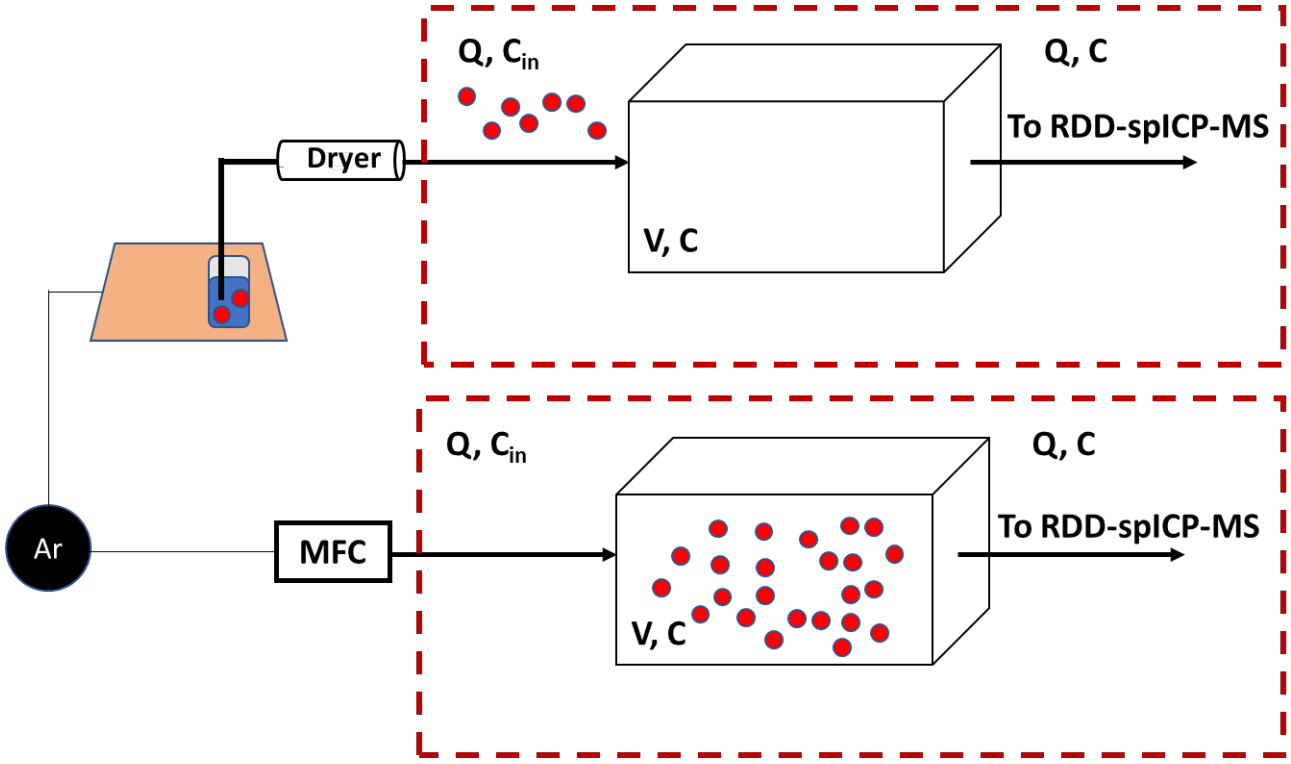

Figure S4 – Schematic representation of the proposed method for time-resolved single metallic NPs characterization during one phase association (top) and one phase decay (bottom) process inside a glove box.

After injecting for 45 min, when the PNC gradually gets stable into a plateau, the AG will be turned off and switch from the association mode into decay mode. As is shown in Figure S4 (bottom), in the decay mode, the NPs have been already homogenously distributed inside the glove box at the starting time. 0.9 L/min pure argon controlled by the MFC will flush out the NPs from the glove box into the RDD-spICP-MS. Similar to the association mode, spICP-MS would record for 2 min, at a time interval of 5 min, to obtain the PSD and PNC. The DR in RDD will be adjusted manually based on the last measurement to fulfil the optimal PNC for

characterizing NPs by spICP-MS. In theory, the concentration inside the glove box and transferred to RDD-spICP-MS will follow the one-phase decay process, which is presented in **Equation S3**.

$$\frac{dC}{dt} = -C \times \frac{Q}{V} \qquad \textbf{Equation S3}$$

After the integration of the time, the time-resolved number concentration of NPs in the glove box could be expressed as **Equation S4**.

$$C = C_0 \times e^{-\frac{Q}{V}t} \qquad \textbf{Equation S4}$$

Where C_0 is the initial PNC of NPs inside the glove box.

As shown in Figure S5a, during the association process, the number concentration of AgNPs increased during that time. The particle size remained always around 100 nm, indicating that there was no obvious aggregation happening in the gas phase inside the glove box and during the transfer from glove box to the ICP-MS. When considering the time evolution of the PNC, Figure S5c shows that the PNC first increased sharply and then gradually saturated, close to a plateau. The data fit well with the one-phase association model (Equations S1 and S2, R^2>0.95). The fitting equation was $C\ [\#/L] = 2.45 \times 10^4 \times (1 - e^{-0.1t[min]})$. This indicates the saturation of AgNPs PNC in the glove box towards that of the initial AgNPs PNC in the aerosol after AG, which was 2.45×10^4 #/L. Considering the flow rate of 0.9 L/min, V is around 9 L. This volume was far smaller than the real volume (350 L) of the glovebox, which was due to a non-homogeneous distribution of the NPs inside the glove box at the current flow rate.

After getting saturation of the AgNPs, the introduction of the AG was closed and switched into the pure argon flush still at 0.9 L/min. As shown in Figure S5b, similar to the association process, the particle size of 100 nm AgNPs remained stable also during the decay process. Considering the time evolution, (Figure S5d), the PNC first decreased rapidly and then more and more slowly. These data fit well with the one-phase decay model (Equations S3 and S4, R^2>0.95). The fitting equation could be obtained as $C\ [\#/L] = 2.45 \times 10^4 \times e^{-0.1t[min]}$. Therefore, the initial PNC in the glovebox was equal to the saturation PNC from the association process at 2.45×10^4 #/L. Moreover, during the decay process, with the same flow rate of 0.9 L/min, the volume from the curve fitting was around 9 L as well, indicating the same mixing conditions during the association and decay process.

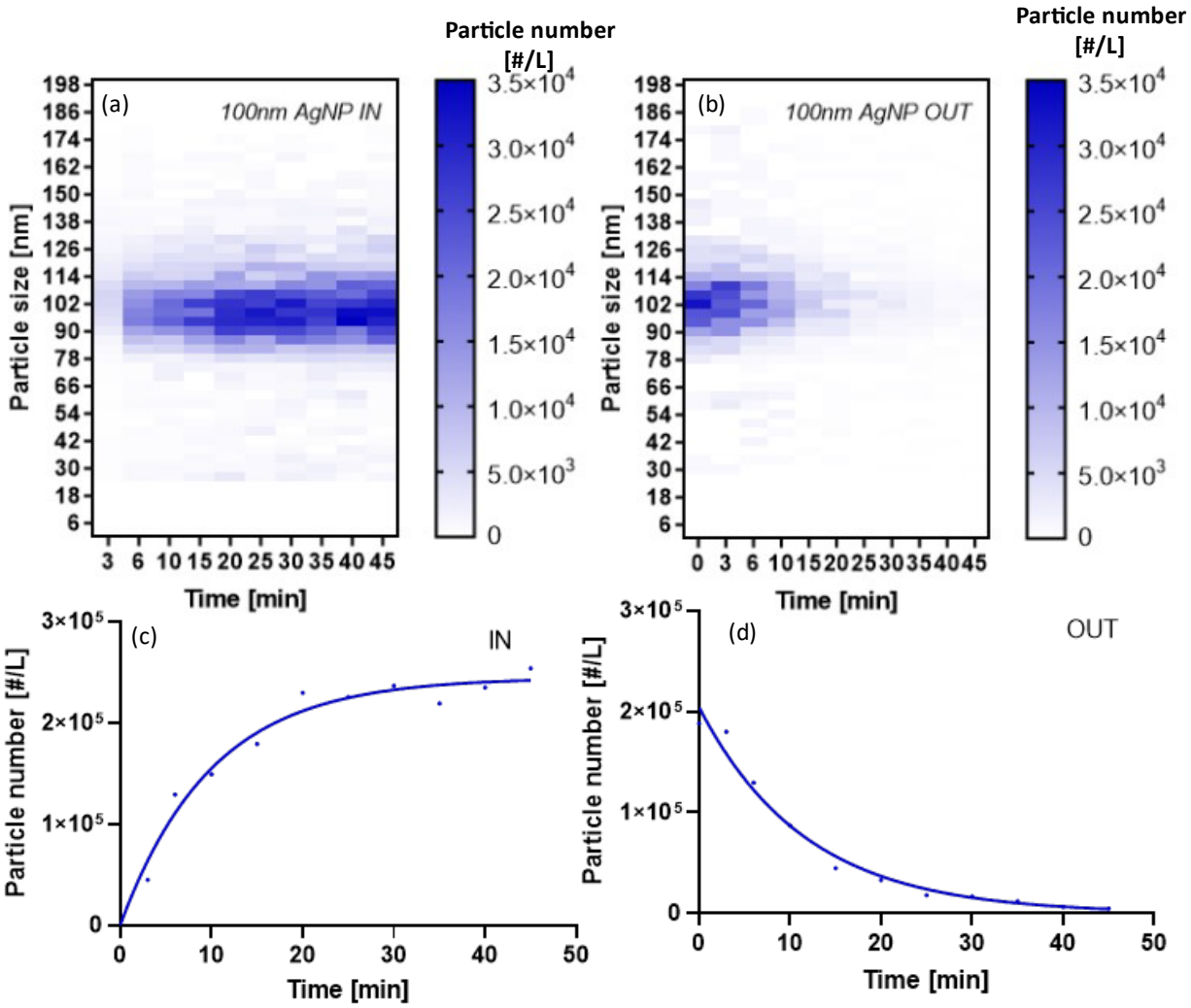

Figure S5 - The time-resolved particle size distribution (a,b) and particle number concentration (c,d) of 100 nm AgNPs in the glove box during the association (a,c) and decay (b,d) processes. One-phase association (c) and one-phase decay (d) models were used for non-linear curve fitting.

4. Particle size calibration

Usually, the calibration of spICP-MS is based on the transport efficiency, which can be calculated by three methods including waste collection, particle size, and particle frequency methods[5], where the waste collection method is hardly used due to its high variation for determining the transport efficiency. The limitation of the size and frequency methods are the scarce availability of standards or CRMs of well-characterized NPs. Recently some new calibration methods were developed without considering transport efficiency including standard addition calibration method[6], instrumental conditions method[7], and microdroplet method[8]. However, all of the methods above start from the liquid standard, which cannot be directly applied to aerosol characterization. Therefore, in this case, direct size calibration methods were built up based on the size selected by DMA.

As confirming the shape and elemental composition of NPs with TEM measurements (Figure S2), a calibration curve was built up between the cubic root of median intensity in spICP-MS and the size selected by DMA, since the peak intensity is proportional to particle mass rather than size. A linear fitting was applied between the cubic root of peak intensity and the selected size (Figure S6). For both AgNPs and CuNPs, the results from DMA and spICP-MS fit quite well for a particle size below 200 nm, indicating a good NP characterization at smaller sizes in DMA-spICP-MS. When the size selected in DMA is larger than 200 nm, the intensity obtained in spICP-MS was below the expected value. This may be due to the different mechanisms of obtaining particle size in DMA and spICP-MS. The size selected by DMA was based on the electrical mobility size, while spICP-MS provided a mass equivalent size.

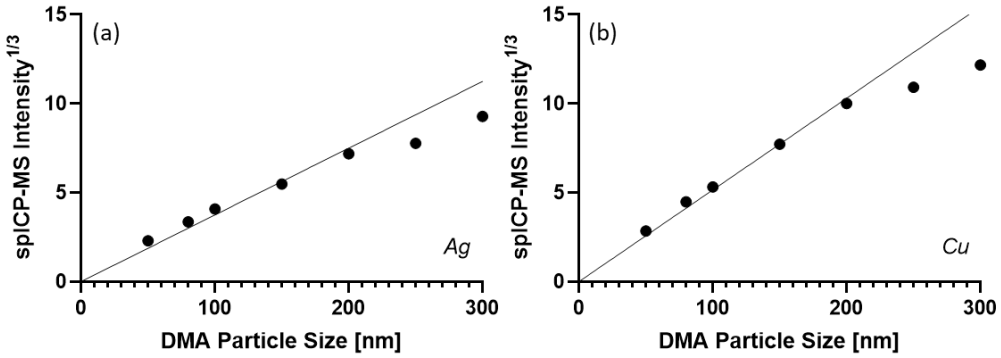

153

154 Figure S6 - The calibration curve between the cubic root of spICP-MS intensity and DMA

155 selected particle size of AgNPs (a) and CuNPs(b).

156

5. Selected area electron diffraction (SAED)

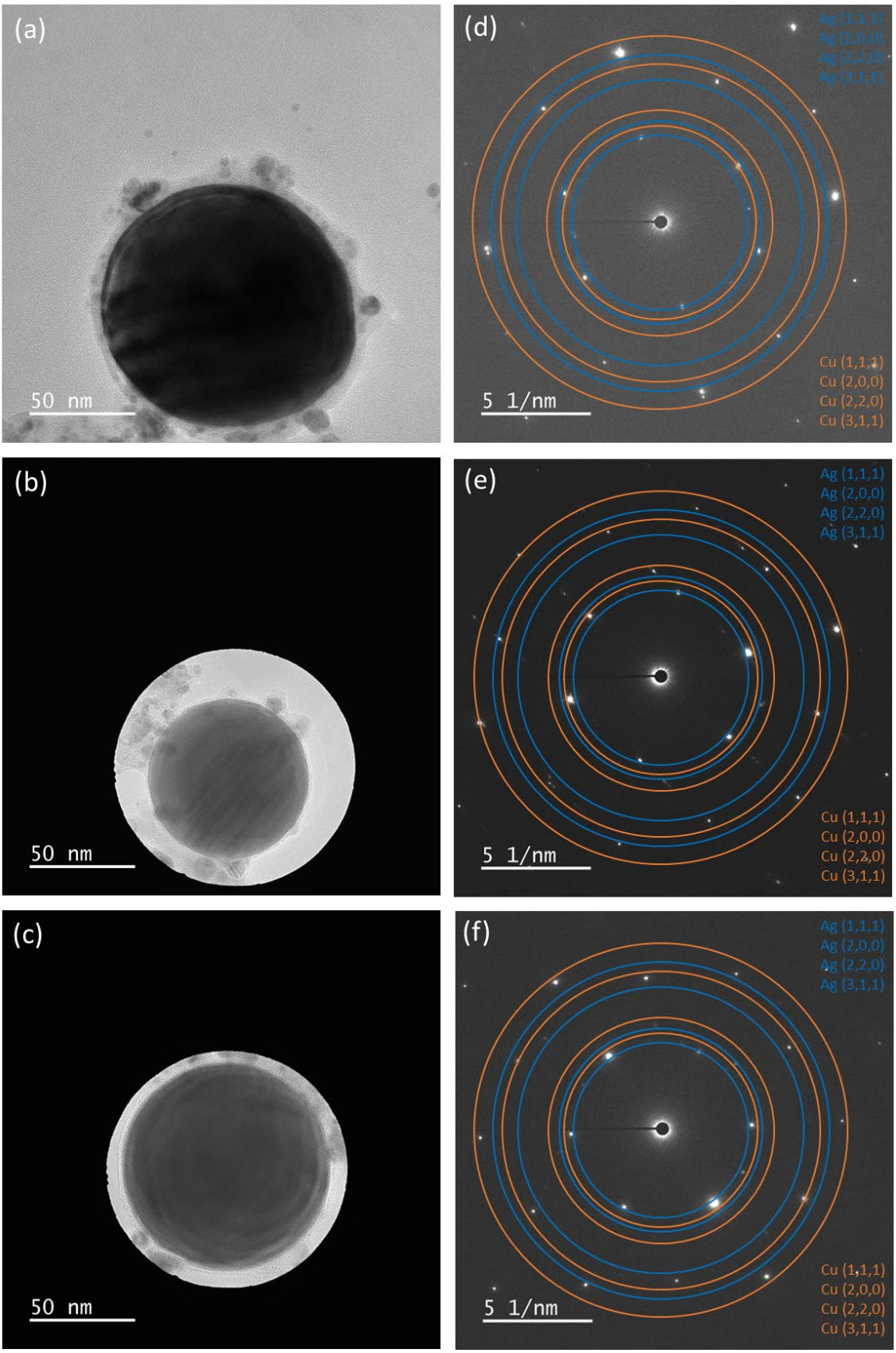

Figure S7 – TEM images (a-c) and selected area electron diffraction (SAED; d-f) of NPs collected offline after the explosion of AgN_3 and CuN_6 mixture in the glove box.

6. Estimated nucleation work

Assuming the classical nucleation theory (CNT) applicable in the condensation of liquid droplet of metal from gas phase, the nucleation work, i.e., the activation energy barrier to overcome in order to generate a liquid spherical droplet from a homogeneous gaseous phase, has the **Equation S5**[9]

$$\Delta G^*_{homo} = \frac{4}{27}\frac{\varepsilon_A^3}{\varepsilon_V^2}\frac{\nu^2\gamma^3}{k_B^2 T^2 \ln^2 S} = \alpha\, \nu^2\gamma^3 \quad \textbf{Equation S5}$$

where ε_A and ε_V are geometrical factors, k_B is the Boltzmann constant, T the temperature, S the saturation, α the cumulative values of the symbols except γ, the surface energy, and ν, the molecular volume.

Assuming α a constant value when comparing homogeneous nucleation work of Ag or Cu nanodroplets from gas phase during the fast quenching from the explosion temperature to room temperature, and estimating the value for γ and ν [10]

$$\gamma_{Ag} = 1.25\, J\, m^{-2}$$

$$\gamma_{Cu} = 1.80\, J\, m^{-2}$$

$$\nu_{Ag} = 1.71\ 10^{-29}\, m^3\, molec$$

177 $v_{Cu} = 1.18\ 10^{-29}\ m^3\ molec$

178 the estimated nucleation works for Ag and Cu nucleation correspond to

179 $\Delta G^*_{homo,Ag} = \alpha \cdot 9.67\ 10^{-60}$

180 $\Delta G^*_{homo,Cu} = \alpha \cdot 13.14\ 10^{-60}$

181 which may allow estimating that Ag requires a lower energy barrier (namely 36% lower)
182 compared to Cu. Thus, we may speculate that nucleation rate of Ag is probably faster than
183 nucleation rate of Cu. This consideration may support the experimental observation of
184 particles with a prevalence of Ag in the core and Cu in the shell.

185

186 Reference

187 1. Foppiano, D., Tarik, M., Müller Gubler, E. & Ludwig, C. Emissions of Secondary
188 Formed ZnO Nano-Objects from the Combustion of Impregnated Wood. An Online
189 Size-Resolved Elemental Investigation. *Environ. Sci. Technol.* **52**, 895–903 (2018).

190 2. R'Mili, B., Le Bihan, O. L. C., Dutouquet, C., Aguerre-Charriol, O. & Frejafon, E.
191 Particle sampling by TEM grid filtration. *Aerosol Sci. Technol.* **47**, 767–775 (2013).

192 3. Cen, T. *et al.* Dilution versus fractionation: Separation technologies hyphenated with
193 spICP-MS for characterizing metallic nanoparticles in aerosols. *J. Aerosol Sci.* 106317
194 (2023).

195 4. Cen, T., Torrent, L., Testino, A. & Ludwig, C. Rotating disk diluter hyphenated with
196 single particle ICP-MS as an online dilution and sampling platform for metallic
197 nanoparticles characterization in ambient aerosol. *J. Aerosol Sci.* 106283 (2023)
198 doi:https://doi.org/10.1016/j.jaerosci.2023.106283.

199 5. Pace, H. E. *et al.* Determining transport efficiency for the purpose of counting and
200 sizing nanoparticles via single particle inductively coupled plasma mass spectrometry.
201 *Anal. Chem.* **83**, 9361–9369 (2011).

202 6. Aramendía, M. *et al.* A novel approach for adapting the standard addition method to
203 single particle-ICP-MS for the accurate determination of NP size and number
204 concentration in complex matrices. *Anal. Chim. Acta* 339738 (2022)
205 doi:10.1016/j.aca.2022.339738.

206 7. Moreira-Álvarez, B., Cid-Barrio, L., Calderón-Celis, F., Costa-Fernández, J. M. &
207 Encinar, J. R. Relative and Transport Efficiency-Independent Approach for the
208 Determination of Nanoparticle Size Using Single-Particle ICP-MS. *Anal. Chem.*

(2023) doi:10.1021/acs.analchem.3c01823.

8. Gundlach-Graham, A. & Mehrabi, K. Monodisperse microdroplets: a tool that advances single-particle ICP-MS measurements. *J. Anal. At. Spectrom.* **35**, 1727–1739 (2020).

9. Nielsen, A. E. *Kinetics of precipitation*. (1964).

10. Vitos, L., Ruban, A. V, Skriver, H. L. & Kollár, J. The surface energy of metals. *Surf. Sci.* **411**, 186–202 (1998).